

# Seven temperate terrestrial planets around the nearby ultracool dwarf star TRAPPIST-1

Michaël Gillon<sup>1</sup>, Amaury H. M. J. Triaud<sup>2</sup>, Brice-Olivier Demory<sup>3,4</sup>, Emmanuël Jehin<sup>1</sup>, Eric Agol<sup>5,6</sup>, Katherine M. Deck<sup>7</sup>, Susan M. Lederer<sup>8</sup>, Julien de Wit<sup>9</sup>, Artem Burdanov<sup>1</sup>, James G. Ingalls<sup>10</sup>, Emeline Bolmont<sup>11,12</sup>, Jeremy Leconte<sup>13</sup>, Sean N. Raymond<sup>13</sup>, Franck Selsis<sup>13</sup>, Martin Turbet<sup>14</sup>, Khalid Barkaoui<sup>15</sup>, Adam Burgasser<sup>16</sup>, Matthew R. Burleigh<sup>17</sup>, Sean J. Carey<sup>10</sup>, Aleksander Chaushev<sup>17</sup>, Chris M. Copperwheat<sup>18</sup>, Laetitia Delrez<sup>1,4</sup>, Catarina S. Fernandes<sup>1</sup>, Daniel L. Holdsworth<sup>19</sup>, Enrico J. Kotze<sup>20</sup>, Valérie Van Grootel<sup>1</sup>, Yaseen Almléay<sup>21,22</sup>, Zouhair Benkhaldoun<sup>15</sup>, Pierre Magain<sup>1</sup> & Didier Queloz<sup>4,23</sup>

**One aim of modern astronomy is to detect temperate, Earth-like exoplanets that are well suited for atmospheric characterization. Recently, three Earth-sized planets were detected that transit (that is, pass in front of) a star with a mass just eight per cent that of the Sun, located 12 parsecs away<sup>1</sup>. The transiting configuration of these planets, combined with the Jupiter-like size of their host star—named TRAPPIST-1—makes possible in-depth studies of their atmospheric properties with present-day and future astronomical facilities<sup>1–3</sup>. Here we report the results of a photometric monitoring campaign of that star from the ground and space. Our observations reveal that at least seven planets with sizes and masses similar to those of Earth revolve around TRAPPIST-1. The six inner planets form a near-resonant chain, such that their orbital periods (1.51, 2.42, 4.04, 6.06, 9.1 and 12.35 days) are near-ratios of small integers. This architecture suggests that the planets formed farther from the star and migrated inwards<sup>4,5</sup>. Moreover, the seven planets have equilibrium temperatures low enough to make possible the presence of liquid water on their surfaces<sup>6–8</sup>.**

Among the three initially reported TRAPPIST-1 planets, one of them—called ‘TRAPPIST-1d’ in the discovery publication<sup>1</sup>—was identified on the basis of only two transit signals, observed at a moderate signal-to-noise ratio. The second transit signal, blended with a transit signal from planet c, was also observed with the High Acuity Widefield K-band Imager (HAWK-I), an infrared imager mounted on the Very Large Telescope (VLT) in Chile. When we analysed the VLT/HAWK-I data—after we submitted the discovery paper—we uncovered a light curve of high enough precision to firmly reveal the triple nature of the observed eclipse (Extended Data Fig. 1). This intriguing result motivated us to intensify our photometric follow-up of the star; this resumed in February and March 2016, with observations of six possible transit windows of TRAPPIST-1d with the Spitzer Space Telescope. Follow-up continued in May 2016 with intense ground-based observations of the star, using the TRAPPIST-South telescope in Chile, its newly commissioned northern twin—TRAPPIST-North—in Morocco, the 3.8-metre UK InfraRed Telescope (UKIRT) in Hawaii, the 4-metre William Herschel and the 2-metre Liverpool telescopes at La Palma, Spain, and the South African Astronomical

Observatory 1.0-metre telescope. Our photometric campaign culminated on 19 September 2016 with the start of a 20-day, nearly continuous monitoring of the star by the Spitzer Space Telescope at a wavelength of 4.5  $\mu\text{m}$ .

The light curves obtained before 19 September 2016 enabled us to discard the 11 possible periods of TRAPPIST-1d that we inferred previously<sup>1</sup>, indicating that the two observed transits originated from different objects. Furthermore, these light curves showed several transit-like signals of unknown origins that we could not relate to a single period (Extended Data Figs 2, 3). The situation was resolved with the 20-day photometric monitoring of the star by Spitzer. The resulting light curve shows 34 clear transits (Fig. 1), which—when combined with the ground-based dataset—enabled us to unambiguously identify four periodic transit signals of periods 4.04 days, 6.06 days, 8.1 days and 12.3 days. These signals correspond to four new transiting planets, named, respectively, TRAPPIST-1d, TRAPPIST-1e, TRAPPIST-1f and TRAPPIST-1g (Fig. 1 and Extended Data Figs 2, 3). This unique solution is supported in several ways: first, enough unique transits were observed per planet (Table 1); second, the shapes of the transit signals were consistent for each planet (see below); and finally, the Spitzer light curve is nearly continuous and its duration was longer than the periods of the four planets. The Spitzer photometry also shows an orphan transit-shaped signal with a depth of around 0.35% and a duration of about 75 minutes, occurring at around Julian Day 2,457,662.55 (Fig. 1); we attribute this signal to a seventh, outermost planet of unknown orbital period—TRAPPIST-1h. We combed our ground-based photometry in search of a second transit of this planet h, but found no convincing match.

We analysed our extensive photometric dataset in three phases. First, we performed individual analyses of all transit light curves with an adaptive Markov chain Monte Carlo (MCMC) code<sup>1,9</sup> to measure their depths, durations and timings (see Methods). We derived a mean transit ephemeris for each planet from their measured transit timings. We successfully checked the consistency of the durations and depths of the transits for planets b to g. For each planet, and especially for f and g, the residuals of the fit show transit timing variations (TTVs) with amplitudes ranging from a few tens of seconds to more

<sup>1</sup>Space Sciences, Technologies and Astrophysics Research (STAR) Institute, Université de Liège, Allée du 6 Août 19C, Bat. B5C, 4000 Liège, Belgium. <sup>2</sup>Institute of Astronomy, Madingley Road, Cambridge CB3 0HA, UK. <sup>3</sup>University of Bern, Center for Space and Habitability, Sidlerstrasse 5, CH-3012 Bern, Switzerland. <sup>4</sup>Cavendish Laboratory, JJ Thomson Avenue, Cambridge CB3 0HE, UK. <sup>5</sup>Astronomy Department, University of Washington, Seattle, Washington 98195, USA. <sup>6</sup>NASA Astrobiology Institute's Virtual Planetary Laboratory, Seattle, Washington 98195, USA. <sup>7</sup>Department of Geological and Planetary Sciences, California Institute of Technology, Pasadena, California 91125, USA. <sup>8</sup>NASA Johnson Space Center, 2101 NASA Parkway, Houston, Texas 77058, USA. <sup>9</sup>Department of Earth, Atmospheric and Planetary Sciences, Massachusetts Institute of Technology, 77 Massachusetts Avenue, Cambridge, Massachusetts 02139, USA. <sup>10</sup>Spitzer Science Center, California Institute of Technology, 1200 E California Boulevard, Mail Code 314-6, Pasadena, California 91125, USA. <sup>11</sup>Naxys, Department of Mathematics, University of Namur, 8 Rempart de la Vierge, 5000 Namur, Belgium. <sup>12</sup>Laboratoire AIM Paris-Saclay, CEA/DRF-CNRS-Univ. Paris Diderot - IRFU/SAP, Centre de Saclay, F-91191 Gif-sur-Yvette Cedex, France. <sup>13</sup>Laboratoire d'astrophysique de Bordeaux, Université Bordeaux, CNRS, B18N, Allée Geoffroy Saint-Hilaire, F-33615 Pessac, France. <sup>14</sup>Laboratoire de Météorologie Dynamique, Sorbonne Universités, UPMC Univ Paris 06, CNRS, 4 Place Jussieu, 75005 Paris, France. <sup>15</sup>Laboratoire LPHEA, Oukaimeden Observatory, Cadi Ayyad University/FSSM, BP 2390 Marrakesh, Morocco. <sup>16</sup>Center for Astrophysics and Space Science, University of California San Diego, La Jolla, California 92093, USA. <sup>17</sup>Leicester Institute for Space and Earth Observation, Department of Physics and Astronomy, University of Leicester, Leicester LE1 7RH, UK. <sup>18</sup>Astrophysics Research Institute, Liverpool John Moores University, Liverpool L3 5RF, UK. <sup>19</sup>Jeremiah Horrocks Institute, University of Central Lancashire, Preston PR1 2HE, UK. <sup>20</sup>South African Astronomical Observatory, PO Box 9, Observatory, 7935, South Africa. <sup>21</sup>Space and Astronomy Department, Faculty of Science, King Abdulaziz University, 21589 Jeddah, Saudi Arabia. <sup>22</sup>King Abdullah Centre for Crescent Observations and Astronomy, Makkah Clock, Mecca 24231, Saudi Arabia. <sup>23</sup>Observatoire de Genève, Université de Genève, 51 chemin des Maillettes, CH-1290 Sauverny, Switzerland.

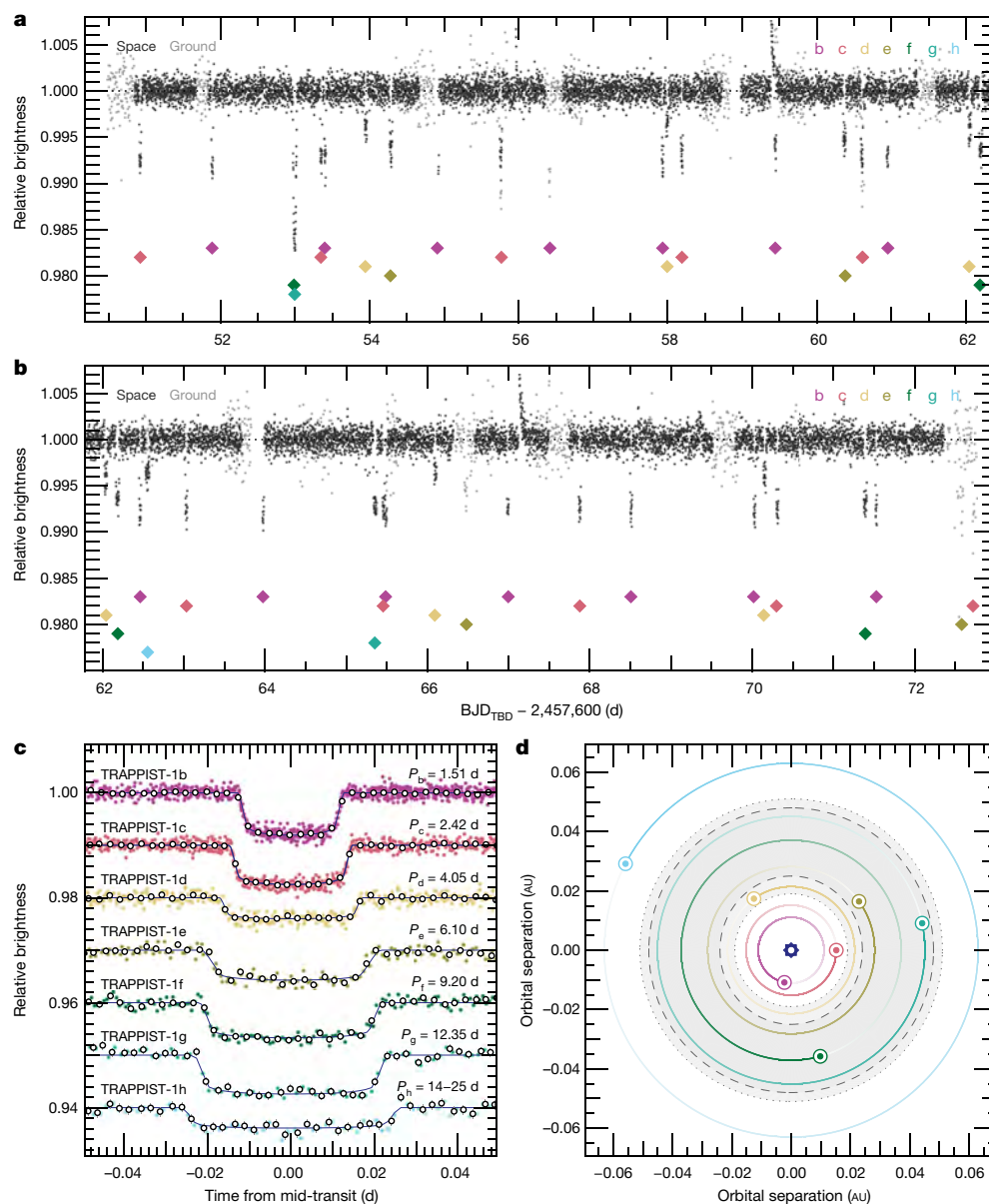


**Figure 1 | The TRAPPIST-1 system as seen by Spitzer.** **a, b,** Top, the dark points represent photometric measurements resulting from the near-continuous observation of the star by the Spitzer Space Telescope from 19 September 2016 to 10 October 2016. The light grey points represent ground-based measurements (binned per 5 minutes for clarity) gathered during gaps in the Spitzer coverage. Coloured diamonds show the positions of the planetary transits. **c,** Period-folded photometric measurements obtained by Spitzer near the transits of planets TRAPPIST-1b to TRAPPIST-1h, corrected for the measured TTVs. Coloured dots show the unbinned measurements; open circles depict binned measurements for visual clarity. The  $1\sigma$  error bars of the binned

measurements are shown as vertical lines. The best-fit transit models are shown as coloured lines. 16, 11, 5, 2, 3, 2 and 1 transits were observed by Spitzer and combined to produce the shown light curves for planets b, c, d, e, f, g and h, respectively. **d,** Representation of the orbits of the seven planets. The colour code matches that in a–c. The grey annulus and the two dashed lines represent the zone around the star in which abundant, long-lived liquid water (that is, oceans) could exist on the surfaces of an Earth-like planet, as estimated under two different assumptions in ref. 6. The relative positions of the planets correspond to their orbital phases during the first transit we detected on this star—a transit by TRAPPIST-1c. The observer is located on the right hand-side of the plot.

than 30 minutes, indicating notable mutual interactions between the planets<sup>10–12</sup> (Extended Data Figs 2, 3).

In a second phase, we carried out a global MCMC analysis of the transits observed by Spitzer to constrain the orbital and physical parameters of the seven planets. We decided to use only the Spitzer data owing to their better precision compared with most of our ground-based data, and because of the minimal amplitude of the limb darkening at  $4.5\mu\text{m}$ ; these factors strengthen the constraints possible on the transit shapes, and thus on the stellar density—and, by extension, on the physical and orbital parameters of the planets<sup>13</sup>. We assumed circular orbits for all of the planets on the basis of the results of *n*-body dynamical simulations, which predicted orbital eccentricities of less than 0.1 for the six inner

planets (Table 1); the orbital eccentricity of the outer planet, h, cannot be constrained from a single transit. This global analysis assumed the *a priori* knowledge of the star that is described in ref. 1 (see Methods). To account for substantial planet–planet interactions, we included TTVs as free parameters for the six inner planets. We used each planet's transit ephemeris (derived in the first phase) as a prior on the orbital solution.

In a third phase, we used the results obtained above to investigate the TTV signals themselves. By performing a series of analytical and numerical *n*-body integrations (see Methods), we could determine initial mass estimates for the six inner planets, along with their orbital eccentricities. We emphasize the preliminary nature of this dynamical

**Table 1 | Updated properties of the TRAPPIST-1 planetary system**

Parameter	Value						
<b>Star</b>	<b>TRAPPIST-1=2MASS J23062928–0502285</b>						
Magnitudes <sup>1</sup>	$V=18.8, R=16.6, I=14.0, J=11.4, K=10.3$						
Distance (pc) <sup>1</sup>	$12.1 \pm 0.4$						
Mass, $M_*$ ( $M_\odot$ ) <sup>†</sup>	$0.0802 \pm 0.0073$						
Radius, $R_*$ ( $R_\odot$ ) <sup>†</sup>	$0.117 \pm 0.0036$						
Density, $\rho_*$ ( $\rho_\odot$ )	$50.7^{+1.2}_{-2.2}$						
Luminosity, $L_*$ ( $L_\odot$ ) <sup>†</sup>	$0.000524 \pm 0.000034$						
Effective temperature, $T_{\text{eff}}$ (K) <sup>†</sup>	$2,559 \pm 50$						
Metallicity, [Fe/H] <sup>†</sup> (dex)	$+0.04 \pm 0.08$						
<b>Planets</b>	<b>b</b>	<b>c</b>	<b>d</b>	<b>e</b>	<b>f</b>	<b>g</b>	<b>h</b>
Number of unique transits observed	37	29	9	7	4	5	1
Period, $P$ (days)	$1.51087081 \pm 0.60 \times 10^{-6}$	$2.4218233 \pm 0.17 \times 10^{-5}$	$4.049610 \pm 0.63 \times 10^{-4}$	$6.099615 \pm 0.11 \times 10^{-4}$	$9.206690 \pm 0.15 \times 10^{-4}$	$12.35294 \pm 0.12 \times 10^{-3}$	$20^{+15}_{-6}$
Mid-transit time, $T_0 - 2,450,000$ (BJD <sub>TDB</sub> )	$7,322.51736 \pm 0.00010$	$7,282.80728 \pm 0.00019$	$7,670.14165 \pm 0.00035$	$7,660.37859 \pm 0.00038$	$7,671.39767 \pm 0.00023$	$7,665.34937 \pm 0.00021$	$7,662.55463 \pm 0.00056$
Transit depth, $(R_p/R_*)^2$ (%)	$0.7266 \pm 0.0088$	$0.687 \pm 0.010$	$0.367 \pm 0.017$	$0.519 \pm 0.026$	$0.673 \pm 0.023$	$0.782 \pm 0.027$	$0.352 \pm 0.0326$
Transit impact parameter, $b$ ( $R_*$ )	$0.126^{+0.092}_{-0.078}$	$0.161^{+0.076}_{-0.084}$	$0.17 \pm 0.11$	$0.12^{+0.11}_{-0.09}$	$0.382 \pm 0.035$	$0.421 \pm 0.031$	$0.45^{+0.22}_{-0.29}$
Transit duration, $W$ (min)	$36.40 \pm 0.17$	$42.37 \pm 0.22$	$49.13 \pm 0.65$	$57.21 \pm 0.71$	$62.60 \pm 0.60$	$68.40 \pm 0.66$	$76.7^{+2.7}_{-2.0}$
Inclination, $i$ (°)	$89.65^{+0.22}_{-0.27}$	$89.67 \pm 0.17$	$89.75 \pm 0.16$	$89.86^{+0.10}_{-0.12}$	$89.680 \pm 0.034$	$89.710 \pm 0.025$	$89.80^{+0.10}_{-0.05}$
Eccentricity, $e$ ( $2\sigma$ upper limit from TTVs)	$<0.081$	$<0.083$	$<0.070$	$<0.085$	$<0.063$	$<0.061$	-
Semi-major axis, $a$ ( $10^{-3}$ AU)	$11.11 \pm 0.34$	$15.21 \pm 0.47$	$21.44^{+0.66}_{-0.63}$	$28.17^{+0.83}_{-0.87}$	$37.1 \pm 1.1$	$45.1 \pm 1.4$	$63^{+27}_{-13}$
Scale parameter, $a/R_*$	$20.50^{+0.16}_{-0.31}$	$28.08^{+0.22}_{-0.42}$	$39.55^{+0.30}_{-0.59}$	$51.97^{+0.40}_{-0.77}$	$68.4^{+0.5}_{-1.0}$	$83.2^{+0.6}_{-1.2}$	$117^{+50}_{-26}$
Irradiation, $S_p$ ( $S_{\text{Earth}}$ )	$4.25 \pm 0.33$	$2.27 \pm 0.18$	$1.143 \pm 0.088$	$0.662 \pm 0.051$	$0.382 \pm 0.030$	$0.258 \pm 0.020$	$0.131^{+0.081}_{-0.067}$
Equilibrium temperature (K) <sup>‡</sup>	$400.1 \pm 7.7$	$341.9 \pm 6.6$	$288.0 \pm 5.6$	$251.3 \pm 4.9$	$219.0 \pm 4.2$	$198.6 \pm 3.8$	$168^{+21}_{-28}$
Radius, $R_p$ ( $R_{\text{Earth}}$ )	$1.086 \pm 0.035$	$1.056 \pm 0.035$	$0.772 \pm 0.030$	$0.918 \pm 0.039$	$1.045 \pm 0.038$	$1.127 \pm 0.041$	$0.755 \pm 0.034$
Mass, $M_p$ ( $M_{\text{Earth}}$ ) (from TTVs)	$0.85 \pm 0.72$	$1.38 \pm 0.61$	$0.41 \pm 0.27$	$0.62 \pm 0.58$	$0.68 \pm 0.18$	$1.34 \pm 0.88$	-
Density, $\rho_p$ ( $\rho_{\text{Earth}}$ )	$0.66 \pm 0.56$	$1.17 \pm 0.53$	$0.89 \pm 0.60$	$0.80 \pm 0.76$	$0.60 \pm 0.17$	$0.94 \pm 0.63$	-

The table shows the values and  $1\sigma$  errors for the parameters of TRAPPIST-1 and its seven planets, as deduced for most parameters from a global analysis of the Spitzer photometry, including *a priori* knowledge of the stellar properties.  $M_*$ ,  $R_*$ ,  $\rho_*$ , and  $L_*$  are the stellar mass, radius, density and luminosity, respectively, given in units of the mass, radius, density or luminosity of the Sun ( $M_\odot$ ,  $R_\odot$ ,  $\rho_\odot$ ,  $L_\odot$ ).  $R_p$ ,  $S_p$ ,  $M_p$  and  $\rho_p$  are respectively the radius, irradiation, mass and density of the planet. BJD<sub>TDB</sub>, barycentric Julian date in the barycentric dynamical time standard. Masses of the planets and upper limits on their eccentricities were deduced from the analysis of the TTVs (see text and Methods). We note that the planet TRAPPIST-1d does not correspond to the discarded ‘TRAPPIST-1d’ candidate presented in ref. 1 (see text).

<sup>†</sup>Informative prior probability distribution functions were assumed for these stellar parameters (see Methods).

<sup>‡</sup>Assuming a null Bond albedo.

solution, which may not correspond to a global minimum of the parameter space, and that additional transit observations of the system will be required to lift the existing degeneracies (see Methods).

Table 1 shows the main planetary parameters derived from our data analysis. We find that five planets (b, c, e, f and g) have sizes similar to that of Earth, while the other two (d and h) are intermediate in size between Mars (which has a radius about half that of Earth) and Earth. The mass estimates for the six inner planets broadly suggest rocky compositions<sup>14</sup> (Fig. 2a). The precision of these mass estimates is not high enough to constrain the fraction of volatiles in the planets’ compositions, except for planet f, whose low density suggests a volatile-rich composition. The volatile content of the planets could be in the form of an ice layer and/or an atmosphere—something that can be verified with follow-up observations during transit with space telescopes such as Hubble<sup>2</sup> and James Webb<sup>3</sup>. We note that the ratio of masses between the six inner planets and TRAPPIST-1 is around 0.02%, as is that of the Galilean satellites and Jupiter, maybe implying a similar formation history<sup>15,16</sup>.

The derived planetary orbital inclinations are all very close to 90°, indicating a dramatically co-planar system seen nearly edge-on. Furthermore, the six inner planets form the longest known near-resonant chain of exoplanets, with the ratios of the orbital periods ( $P$ )  $P_c/P_b$ ,  $P_d/P_c$ ,  $P_e/P_d$ ,  $P_f/P_e$  and  $P_g/P_f$  being close to the ratios of small integers, namely 8/5, 5/3, 3/2, 3/2 and 4/3, respectively. This proximity to mean motion resonances of several planet pairs explains the substantial amplitudes of the measured TTVs. Similar near-resonant chains involving up to four planets have been discovered in compact systems

containing super-Earths and Neptunes orbiting Sun-like stars<sup>5,17</sup>. Orbital resonances are naturally generated when multiple planets interact within their nascent gaseous discs<sup>18</sup>. The favoured theoretical scenario for the origin of the TRAPPIST-1 system involves accretion of the planets further from the star, followed by a phase of disc-driven inward migration<sup>4,19</sup>—a process first studied in the context of the Galilean moons around Jupiter<sup>20</sup>. The planets’ compositions should reflect their formation zone, so this scenario predicts that the planets should be volatile-rich and have lower densities than Earth<sup>21,22</sup>, in good agreement with our preliminary result for planet f (Fig. 2a).

The stellar irradiation of the planets covers a range from about  $4.3S_{\text{Earth}}$  to around  $0.13S_{\text{Earth}}$  (where  $S_{\text{Earth}}$  is the solar irradiation at 1 AU); this is very similar to the range seen in the inner Solar System (Mercury,  $6.7S_{\text{Earth}}$ ; Ceres,  $0.13S_{\text{Earth}}$ ). Notably, planets c, d and f have stellar irradiances very close to those of Venus, Earth and Mars, respectively (Fig. 2). However, even at these low insulations, all seven planets are expected to be either tidally synchronized<sup>23</sup>, or trapped in a higher-order spin-orbit resonance, the latter being rather unlikely considering the constraints on the orbital eccentricities<sup>24</sup> (Table 1). Using a one-dimensional cloud-free climate model that accounts for the low-temperature spectrum of the host star<sup>25</sup>, we deduce that planets e, f and g could harbour water oceans on their surfaces, assuming Earth-like atmospheres. The same inference is obtained when running a three-dimensional climate model<sup>26</sup>, assuming that the planets are tidally synchronous. For the three inner planets (b, c and d), our three-dimensional climate modelling results in a runaway greenhouse scenario. The cloud feedback that usually decreases the surface



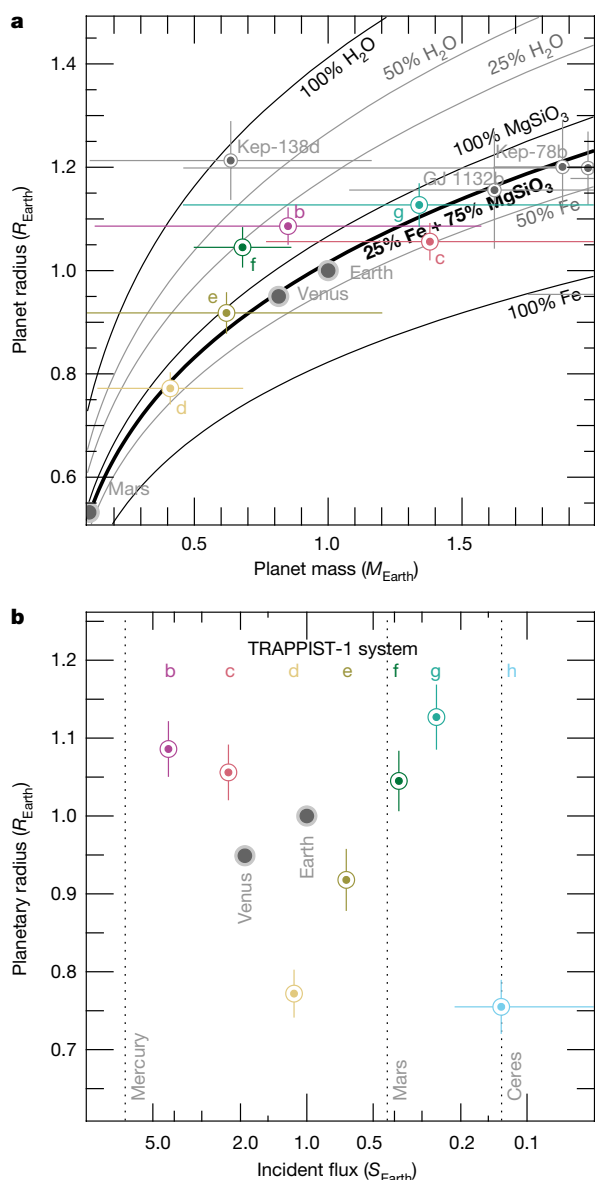


**Figure 2 | Mass-radius and incident-flux-radius diagrams for terrestrial planets.** In both panels, the coloured circular symbols represent the TRAPPIST-1 planets, and the horizontal and vertical lines are  $1\sigma$  error bars. **a**, Relationship between mass and radius for planets of between 0.5 and 1.5 Earth radii, and between 0.1 and 2 Earth masses. The solid lines represent theoretical mass-radius curves<sup>14</sup> for planets with different compositions. The fiducial model is 100% MgSiO<sub>3</sub> (rock), whose fractional part decreases either with an increasing fraction of water (the radius increases), or with increasing fractions of iron (the radius decreases). **b**, Planetary radii are plotted against incident flux. Venus and Earth are shown as grey circles, and Mercury, Mars and Ceres as dotted vertical lines. There are larger errors in the irradiation of the planet TRAPPIST-1h, because its orbital period is unknown.

temperatures for synchronous planets is rather inefficient for such short-period objects<sup>27</sup>. Nevertheless, if some water survived the hot early phase of the system<sup>28</sup>, the irradiation received by planets b, c and d is still low enough to make it possible for limited regions on their surfaces to harbour liquid water<sup>1,7</sup>. As for planet h, although its orbital period and therefore its distance from its star are not yet well defined, its irradiation is probably too low to sustain surface temperatures above the melting point of water. However, it could still harbour surface liquid water if it has enough internal energy—for example, from tidal heating—or if a large fraction of its primordial hydrogen-rich atmosphere has survived, which could strongly slow down the loss of its internal heat<sup>8</sup>.

We found the long-term dynamical evolution of the system to be highly dependent on the exact orbital parameters and masses of the seven planets, which are at present too uncertain to make possible any reliable predictions (see Methods). All of our dynamical simulations predict small but non-zero orbital eccentricities for the six inner planets (see the  $2\sigma$  upper limits in Table 1). The resulting tidal heating could be strong enough to substantially affect their energy budgets and geological activities<sup>29</sup>.

The TRAPPIST-1 system is a compact analogue of the inner Solar System (Fig. 2b). It represents a unique opportunity to thoroughly characterize<sup>1–3</sup> temperate Earth-like planets that are orbiting a much cooler and smaller star than the Sun, and, notably, to study the impact of tidal locking<sup>22</sup>, tidal heating<sup>29</sup>, stellar activity<sup>22</sup> and an extended pre-main-sequence phase<sup>30</sup> on their atmospheric properties.

**Online Content** Methods, along with any additional Extended Data display items and Source Data, are available in the online version of the paper; references unique to these sections appear only in the online paper.

Received 21 November; accepted 21 December 2016.

- Gillon, M. *et al.* Temperate Earth-sized planets transiting a nearby ultracool dwarf star. *Nature* **533**, 221–224 (2016).
- de Wit, J. *et al.* A combined transmission spectrum of the Earth-sized exoplanets TRAPPIST-1 b and c. *Nature* **537**, 69–72 (2016).
- Barstow, J. K. & Irwin, P. G. J. Habitable worlds with JWST: transit spectroscopy of the TRAPPIST-1 system? *Mon. Not. R. Astron. Soc.* **461**, L92–L96 (2016).
- Cresswell, P. & Nelson, R. P. On the evolution of multiple protoplanets embedded in a protostellar disc. *Astron. Astrophys.* **450**, 833–853 (2006).
- Mills, S. M. *et al.* A resonant chain of four transiting, sub-Neptune planets. *Nature* **533**, 509–512 (2016).
- Kopparapu, R. K. *et al.* Habitable zones around main-sequence stars: new estimates. *Astrophys. J.* **765**, 131 (2013).
- Leconte, J. *et al.* 3D climate modelling of close-in land planets: circulation patterns, climate moist instability, and habitability. *Astron. Astrophys.* **554**, A69 (2013).
- Stevenson, D. J. Life-sustaining planets in interstellar space? *Nature* **400**, 32 (1999).
- Gillon, M. *et al.* The TRAPPIST survey of southern transiting planets. I. Thirty eclipses of the ultra-short period planet WASP-43 b. *Astron. Astrophys.* **542**, A4 (2012).
- Agol, E., Steffen, J., Sari, R. & Clarkson, W. On detecting terrestrial planets with timing of giant planet transits. *Mon. Not. R. Astron. Soc.* **359**, 567–579 (2005).
- Holman, M. J. & Murray, N. W. The use of transit timing to detect terrestrial-mass extrasolar planets. *Science* **307**, 1288–1291 (2005).
- Fabrycky, D. C. in *Exoplanets* (ed. Seager, S.) 217–238 (Univ. Arizona Press, 2010).
- Winn, J. N. in *Exoplanets* (ed. Seager, S.) 55–77 (Univ. Arizona Press, 2010).
- Zeng, L., Sasselov, D. D. & Jacobsen, S. B. Mass-radius relation for rocky planets based on PREM. *Astrophys. J.* **819**, 127 (2016).
- Chiang, E. & Laughlin, G. The minimum-mass extrasolar nebula: in situ formation of close-in super-Earths. *Mon. Not. R. Astron. Soc.* **431**, 3444–3455 (2013).
- Kane, S. R., Hinkel, N. R. & Raymond, S. N. Solar system moons as analogs for compact exoplanetary systems. *Astron. J.* **146**, 122 (2013).
- MacDonald, M. G. *et al.* A dynamical analysis of the Kepler-80 system of five transiting planets. *Astron. J.* **152**, 105 (2016).
- Papaloizou, J. C. B. & Szuszkiewicz, E. On the migration-induced resonances in a system of two planets with masses in the Earth mass range. *Mon. Not. R. Astron. Soc.* **363**, 153–176 (2005).
- Terquem, C. & Papaloizou, J. C. B. Migration and the formation of systems of hot super-Earths and Neptunes. *Astrophys. J.* **654**, 1110–1120 (2007).
- Goldreich, P. & Tremaine, S. Disk-satellite interactions. *Astrophys. J.* **241**, 425–441 (1980).
- Raymond, S. N., Barnes, R. & Mandell, A. M. Observable consequences of planet formation models in systems with close-in terrestrial planets. *Mon. Not. R. Astron. Soc.* **384**, 663–674 (2008).
- Alibert, Y. & Benz, W. Formation and composition of planets around very low mass stars. *Astron. Astrophys.* **598**, L5 (2017).
- Kasting, J. F., Whitmire, D. P. & Reynolds, R. T. Habitable zones around main-sequence stars. *Icarus* **101**, 108–128 (1993).
- Ribas, I. *et al.* The habitability of Proxima Centauri b. I. Irradiation, rotation and volatile inventory from formation to the present. *Astron. Astrophys.* **596**, A111 (2016).
- Wordsworth, R. D. *et al.* Is Gliese 581d habitable? Some constraints from radiative-convective climate modeling. *Astron. Astrophys.* **522**, A22 (2010).
- Turbet, M. *et al.* The habitability of Proxima Centauri b II. Possible climates and observability. *Astron. Astrophys.* **596**, A112 (2016).

27. Kopparapu, R. K. *et al.* The inner edge of the habitable zone for synchronously rotating planets around low-mass stars using general circulation models. *Astrophys. J.* **819**, 84 (2016).
28. Bolmont, E. *et al.* Water loss from Earth-sized planets in the habitable zones of ultracool dwarfs: implications for the planets of TRAPPIST-1. *Mon. Not. R. Astron. Soc.* **464**, 3728–3741 (2017).
29. Barnes, R. *et al.* Tidal limits to planetary habitability. *Astrophys. J.* **700**, L30–L33 (2009).
30. Luger, R. & Barnes, R. Extreme water loss and abiotic O<sub>2</sub> buildup on planets throughout the habitable zone of M dwarfs. *Astrobiol.* **15**, 119–143 (2015).

**Acknowledgements** This work is based in part on observations made with the Spitzer Space Telescope, which is operated by the Jet Propulsion Laboratory, California Institute of Technology, under a contract with NASA. The material presented here is based on work supported in part by NASA under contract no. NNX15AI75G. TRAPPIST-South is a project funded by the Belgian Fonds (National) de la Recherche Scientifique (F.R.S.-FNRS) under grant FRFC 2.5.594.09.F, with the participation of the Swiss National Science Foundation (FNS/SNSF). TRAPPIST-North is a project funded by the University of Liège, and performed in collaboration with Cadi Ayyad University of Marrakesh. The research leading to these results has received funding from the European Research Council (ERC) under the FP/2007-2013 ERC grant agreement no. 336480, and under the H2020 ERC grant agreement no. 679030; and from an Actions de Recherche Concertée (ARC) grant, financed by the Wallonia–Brussels Federation. The VLT data used in this work were taken under program 296.C-5010(A). UKIRT is supported by NASA and operated under an agreement among the University of Hawaii, the University of Arizona, and Lockheed Martin Advanced Technology Center; operations are enabled through the cooperation of the East Asian Observatory. The Liverpool Telescope is operated on the island of La Palma by Liverpool John Moores University (JMU) in the Spanish Observatorio del Roque de los Muchachos of the Instituto de Astrofísica de Canarias, with financial support from the UK Science and Technology Facilities Council. This paper uses observations made at the South African Astronomical Observatory (SAAO). M.G., E.J. and V.V.G. are F.R.S.-FNRS research associates. B.-O.D. acknowledges support from the Swiss National Science Foundation in the form of a SNSF Professorship (PP00P2\_163967). E.A. acknowledges support from National Science Foundation (NSF) grant AST-1615315, and NASA grants NNX13AF62G and NNX15ZDA001C. E.B. acknowledges that this work is part of the F.R.S.-FNRS ExtraOrdinary research project and acknowledges funding by the European Research Council through ERC grant SPIRE 647383.

S.N.R. thanks the Agence Nationale pour la Recherche (ANR) for support via grant ANR-13-BS05-0003-002 (project MOJO). D.L.H. acknowledges financial support from the UK Science and Technology Facilities Council. The authors thank C. Owen, C. Wolf and the rest of the SkyMapper team for their attempts to monitor the star from Australia; from UKIRT, the director R. Green and the staff scientists W. Varricatt and T. Kerr; the ESO staff at Paranal for their support with the HAWK-I observations; JMU and their flexibility as regards the Liverpool Telescope schedule, which allowed us to search actively for the planets, and to extend our time allocation in the face of amazing results; for the William Herschel Telescope, C. Fariña, F. Riddick, F. Jiménez and O. Vaduvescu for their help and kindness during observations; and for SAOA, the telescopes operations manager R. Sefako for his support.

**Author Contributions** M.G. leads the ultracool dwarf transit survey that uses the TRAPPIST telescope and led the photometric follow-up of the star TRAPPIST-1; he also planned and analysed most of the observations, led their scientific exploitation, and wrote most of the manuscript. A.H.M.J.T. led the observational campaign using the La Palma telescopes (the Liverpool Telescope, LT, and William Herschel Telescope, WHT). C.M.C. managed the scheduling of the LT observations, and Ar.B. performed the photometric analysis of the resulting LT and WHT images. B.-O.D. led the TTV/dynamical simulations. E.A. and K.M.D. performed independent analyses of the transit timings. J.G.I. and S.J.C. helped to optimize the Spitzer observations. B.-O.D., J.G.I. and J.d.W. performed independent analyses of the Spitzer data. M.G., E.J., L.D., Ar.B., P.M., K.B., Y.A. and Z.B. performed the TRAPPIST observations and their analysis. S.M.L. obtained the director's discretionary time on UKIRT, and, with E.J., managed the preparation of the UKIRT observations. M.T., J.L., F.S., E.B. and S.N.R. carried out atmospheric modelling for the planets and worked on the theoretical interpretation of their properties. V.V.G. managed the SAOA observations performed by C.S.F., M.R.B., D.L.H., A.C. and E.J.K. All co-authors assisted with writing the manuscript. A.H.M.J.T. prepared most of the figures.

**Author Information** Reprints and permissions information is available at [www.nature.com/reprints](http://www.nature.com/reprints). The authors declare no competing financial interests. Readers are welcome to comment on the online version of the paper. Correspondence and requests for materials should be addressed to M.G. ([michael.gillon@ulg.ac.be](mailto:michael.gillon@ulg.ac.be)).

**Reviewer Information** *Nature* thanks D. Deming and I. Snellen for their contribution to the peer review of this work.

## METHODS

**Observations and photometry.** In addition to the ground-based observations described in ref. 1, this work was based on 1,333 hours of new observations gathered from the ground with the 60-cm telescopes TRAPPIST-South (469 h) and TRAPPIST-North (202 h), the 8-m Very Large Telescope (3 h), the 4.2-m William Herschel Telescope (26 h), the 4-m UKIRT (25 h), the 2-m Liverpool Telescope (50 h), and the 1-m SAAO telescope (11 h), and from space with Spitzer (518 h).

The new observations of the star gathered by the TRAPPIST-South<sup>1,31,32</sup> 60-cm telescope (La Silla Observatory, Chile) occurred on the nights of 29 December 2015 to 31 December 2015, and from 30 April 2016 to 11 October 2016. The observational strategy used was the same as that described in ref. 1 for previous TRAPPIST-South observations of the star.

TRAPPIST-North<sup>33</sup> is a new 60-cm robotic telescope installed in spring 2016 at Oukaïmeden Observatory in Morocco. It forms an instrumental project led by the University of Liège, in collaboration with the Cadi Ayyad University of Marrakesh, and is, like its southern twin TRAPPIST-South, totally dedicated to observations of exoplanet transits and small bodies of the Solar System. TRAPPIST-North observations of TRAPPIST-1 were performed from 1 June 2016 to 12 October 2016. Each run of observations consisted of 50-s exposures obtained with a thermoelectrically cooled  $2k \times 2k$  deep-depletion charge-coupled-device (CCD) camera (field of view of  $19.8' \times 19.8'$ ; image scale of  $0.61''$  per pixel). The observations used the same 'I+z' filter as for most of the TRAPPIST-South observations<sup>1</sup>.

The new VLT/HAWK-I<sup>34</sup> (Paranal Observatory, Chile) observations that revealed a triple transit of planets c, e and f (see main text and Extended Data Fig. 1) were performed during the night of 10 December 2015 to 11 December 2015, with the observational strategy described in ref. 1 (NB2090 filter), except that each exposure was composed of 18 integrations of 2 s.

The 4-m telescope UKIRT (Mauna Kea, Hawaii) and its Wide-Field Camera (WFCAM), an infrared camera<sup>35</sup>, observed the star on 24 June, 16, 18, 29 and 30 July, and 1 August 2016. Here, too, the observational strategy was the same as used as in previous observations of the star<sup>1</sup> (J filter; exposures of five integrations of 1 s).

The 4.2-m William Herschel Telescope (La Palma, Canary Islands) observed the star for three nights in a row from 23 August 2016 to 25 August 2016 with its optical  $2k \times 4k$  auxiliary-port camera (ACAM)<sup>36</sup>, which has an illuminated circular field of view of diameter  $8'$  and an image scale of  $0.25''$  per pixel. The observations were performed in the Bessel I filter with exposure times of between 15 s and 23 s.

Ten runs of observation of TRAPPIST-1 were performed by the robotic 2-m Liverpool Telescope between June and October 2016. These observations were obtained through a Sloan-z filter with the  $4k \times 4k$  IO:O CCD camera<sup>37</sup> (field of view  $10' \times 10'$ ). A  $2 \times 2$  binning scheme resulted in an image scale of  $0.30''$  per pixel. An exposure time of 20 s was used for all images.

The 1-m telescope at the South African Astronomical Observatory (SAAO, Sutherland, South Africa) observed the star on the nights of 18 to 19 June 2016, 21 to 22 June 2016, and 2 to 3 July 2016. The observations consisted of 55-s exposures taken by the  $1k \times 1k$  Sutherland high-speed optical (SHOC) CCD camera<sup>38</sup> (field of view  $2.85' \times 2.85'$ ) using a Sloan z filter and with a  $4 \times 4$  binning, resulting in an image scale of  $0.67''$  per pixel.

For all ground-based data, a standard pre-reduction (involving bias, dark, flat-field correction) was applied, and then the stellar fluxes were measured from the calibrated images using DAOPHOT aperture photometry software<sup>39</sup>. In a final stage, a selection of stable comparison stars was manually performed in order to obtain the most accurate differential photometry possible for TRAPPIST-1.

The Spitzer Space Telescope observed TRAPPIST-1 using its Infrared Array Camera (IRAC) detector<sup>40</sup> for 5.7 h on 21 February 2016, for 6.5 h on 3, 4, 7, 13, 15 and 18 March 2016, and continuously from 19 September 2016 to 10 October 2016. All of these observations were made at  $4.5 \mu\text{m}$  in subarray mode ( $32 \times 32$  pixel windowing of the detector) with an exposure time of 1.92 s. The observations were made without dithering and in the pointing calibration and reference sensor (PCRS) peak-up mode<sup>41</sup>, which maximizes the accuracy in the position of the target on the detector so as to minimize the so-called pixel phase effect of IRAC indium antimonide arrays<sup>42</sup>. All of the Spitzer data were calibrated with the Spitzer pipeline S19.2.0, and delivered as cubes of 64 subarray images. Our photometric extraction was identical to that described in ref. 43. We used DAOPHOT to measure the fluxes by aperture photometry, and combined the measurements per cube of 64 images. The photometric errors were taken as the errors on the average flux measurements for each cube.

The observations used here are summarized in Extended Data Table 1.

**Photometry analysis.** The total photometric dataset—including the data in ref. 1—consists of 81,493 photometric measurements spread over 351 light curves. We converted each universal time (UT) of mid-exposure to the BJD<sub>TDB</sub> time system<sup>44</sup>. We then performed an individual model selection for each light curve; tested a large range of models composed of a baseline model representing the flux variations correlated to variations of external parameters (for example,

point-spread function size or position on the chip, time or airmass) as low-order (0 to 4) polynomial functions; and eventually added to this baseline model a transit model<sup>45</sup> and/or a flare model (instantaneous flux increase followed by an exponential decrease) if a structure consistent in shape with these astrophysical signals was visible in the light curve (two flares were captured by Spitzer during its 20-day-monitoring campaign; see Fig. 1). The final model of each light curve was selected by minimization of the Bayesian information criterion (BIC)<sup>46</sup>. For all of the Spitzer light curves, we needed to include a linear or quadratic function of the  $x$ - and  $y$ -positions of the point-spread function (PSF) centre (as measured in the images by the fit of a two-dimensional gaussian profile) in the baseline model to account for the pixel phase effect<sup>42,43</sup>, complemented in some light curves by a linear or quadratic function of the measured widths of the PSF in the  $x$ - and/or  $y$ -directions<sup>43</sup>.

For each light curve presenting a transit-like structure whose existence was favoured by the BIC, we explored the posterior probability distribution function (PDF) of its parameters (width, depth, impact parameter and mid-transit timing) with an adaptive MCMC code<sup>1,9</sup>. For the transits originating from the firmly confirmed planets b and c, we fixed the orbital period to the values in ref. 1. For the other transit-like structures, the orbital period was also a free parameter. As in ref. 1, we assumed circular orbits for the planets, and we assumed the normal distributions  $N(0.04, 0.08^2)$  dex,  $N(2,555, 85^2)$  K,  $N(0.082, 0.011^2) M_{\odot}$ , and  $N(0.114, 0.006^2) R_{\odot}$  as prior PDFs for the stellar metallicity, effective temperature, mass, and radius, respectively, on the basis of *a priori* knowledge of the stellar properties<sup>1,47</sup>. We assumed a quadratic limb-darkening law for the star<sup>48</sup>, with coefficients interpolated for TRAPPIST-1 from the tables of ref. 49. Details of the MCMC analysis of each light curve are as in ref. 1.

We used the resulting values for the timings of the transits to identify planetary candidates, by searching for periodicities and consistency between the derived transit shape parameters. Owing to the high precision and near-continuous nature of the photometry acquired by Spitzer in September and October 2016, this process allowed us to firmly identify the four new planets, d, e, f and g, with periods of 4.1 days, 6.1 days, 9.2 days and 12.3 days respectively (Extended Data Figs 2, 3). We then measured updated values for their transit timings through new MCMC analyses of their transit light curves, for which the orbital periods were fixed to the determined values. For the six planets b, c, d, e, f and g, we then performed a linear regression analysis of the measured transit timings,  $T_i$ , as a function of their epochs,  $E_i$ , to derive a transit ephemeris  $T_i = T_0 (\pm \sigma T_0) + E_i \times P (\pm \sigma P)$ , with  $T_0$  being the timing of a reference transit for which the epoch is arbitrarily set to 0,  $P$  being the orbital period, and  $\sigma T_0$  and  $\sigma P$  being their errors as deduced from the co-variance matrix (Table 1). For all planets, the residuals of the fit showed some significant deviation, indicating TTVs, which is unsurprising given the compactness of the system and the near-resonant chain formed by the six inner planets (see below).

For a transit-like signal observed by Spitzer at BJD<sub>TDB</sub>  $\sim 2,457,662.55$  (Fig. 1), the significance of the detection ( $>10\sigma$ ) was large enough to allow us to conclude that a seventh, outermost planet exists as well. This conclusion is based not only on the high significance of the signal and the consistency of its shape with one expected for a planetary transit, but also on the photometric stability of the star at  $4.5 \mu\text{m}$  (outside of the frequent transits and the rare—about one per week—flares) as revealed by Spitzer (Fig. 1).

In a final stage, we performed the global MCMC analysis of the 35 transits observed by Spitzer that is described in the main text. It consisted of two chains of 100,000 steps, whose convergence was successfully checked using the statistical test of ref. 50. The parameters derived from this analysis for the star and its planets are shown in Table 1.

**TTV analysis.** We used the TTV method<sup>10,11</sup> to estimate the masses of the TRAPPIST-1 planets. The continuous exchange of angular momentum between gravitationally interacting planets causes them to accelerate and decelerate along their orbits, making their transit times occur early or late compared with a Keplerian orbit<sup>14</sup>.

All six inner TRAPPIST-1 planets exhibit transit timing variations owing to perturbations from their closest neighbours (Extended Data Fig. 4). The TTV signal for each planet is dominated primarily by interactions with adjacent planets, and these signals have the potential to be particularly large because each planet is near a mean motion resonance with its neighbours. As calculated from the present data, the TTV amplitudes range in magnitude from 2 min to more than 30 min. However, the distance of these pairs to exact resonances controls the amplitude and the period of the TTV signals and is not precisely pinned down by the present dataset. Moreover, the relatively short timeframe during which the transits have been monitored prevents an efficient sampling of the TTV oscillation frequencies for the different pairs of planets, defined by  $f(\text{TTV}) = n_i/P_i - n_j/P_j$ , where  $P$  is the orbital period,  $n$  the mean motion, and  $i$  and  $j$  the planet indices<sup>10</sup>.

We modelled TTVs using both numerical integrations (TTVFast<sup>51</sup> and Mercury<sup>52</sup>) and analytical integrations (TTVFaster<sup>53</sup>) of a system of six gravitationally interacting, co-planar planets. TTVFaster is based on analytical approximations of TTVs derived using perturbation theory and includes all terms at



first order in eccentricity. Furthermore, it includes only those perturbations to a planet from adjacent planets. To account for the 8/5 and 5/3 near-resonances in the system, we also included the dominant terms for these resonances, which appear at second and third order in the eccentricities. We determined these higher-order terms using the results of ref. 54. TTVFaster has the advantage that it is much faster to compute compared with  $n$ -body integrations. It is applicable for this system given the low eccentricities determined via TTV analysis (determined independently with  $n$ -body integrations and self-consistently with TTVFaster).

We used two different minimization techniques: Levenberg–Marquardt<sup>55</sup> and Nelder–Mead<sup>56</sup>. For the purpose of analysis, we used the 98 independent transit times for all six planets and 5 free parameters per planet (mass, orbital period, transit epoch and eccentricity vectors  $e\cos\omega$  and  $e\sin\omega$ , with  $e$  being the eccentricity and  $\omega$  the argument of periastron). We elected not to include the seventh planet, h, in the fit, because only a single transit has been observed and there is not yet an indication of detectable interactions with any of the inner planets. Likewise, we did not detect any perturbation that would require the inclusion of an additional, undetected non-transiting planet in the dynamical fit. The six-planet model provided a good fit to the existing data (Extended Data Fig. 4), and we found no compelling evidence for extending the present model complexity given the existing data.

Our three independent analyses of the same set of transit timings revealed multiple, mildly inconsistent, solutions that fit the data equally well provided that non-circular orbits are allowed in the fit. It is likely that this solution degeneracy originates from the high dimensionality of the parameter space, combined with the limited constraints brought by the present dataset. The best-fit solution that we found—computed with Mercury<sup>52</sup>—has a chi-squared of 92 for 68 degrees of freedom, but involves non-negligible eccentricities (0.03 to 0.05) for all planets, probably jeopardizing the long-term stability of the system. In this context, we decided to present conservative estimates of the planets' masses and upper limits for the eccentricities without favouring one of the three independent analyses. For each parameter, we considered as the  $1\sigma$  lower/upper limits the smallest/largest values of the  $1\sigma$  lower/upper limits of the three posterior PDFs, and the average of the two computed limits as the most representative value. The values and error bars computed for the planets' masses and the  $2\sigma$  upper limits for their orbital eccentricities are given in Table 1.

Additional precise transit timings for all seven planets will be key in constraining further the planet masses and eccentricities and in isolating a unique, well defined, dynamical solution.

**Initial assessment of the system's long-term stability.** We investigated the long-term evolution of the TRAPPIST-1 system using two  $n$ -body integration packages: Mercury<sup>52</sup> and WHFAST<sup>57</sup>. We started from the orbital solution produced in Table 1, and integrated over 0.5 million years (Myr). This corresponds to roughly 100 million orbits for planet b. We repeated this procedure by sampling a number of solutions within the  $1\sigma$  intervals of confidence. Most integrations resulted in the disruption of the system on a 0.5-Myr timescale.

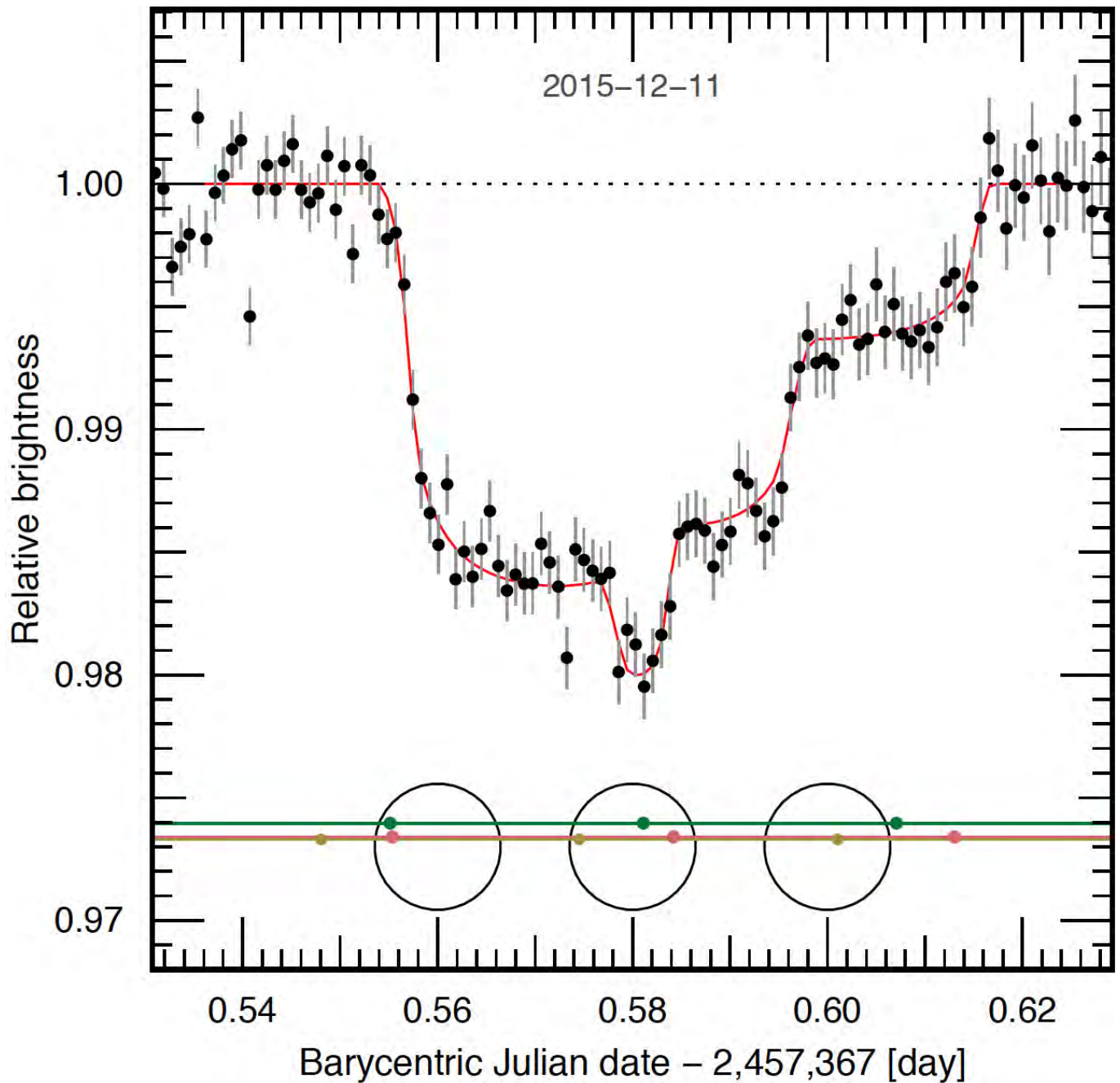
We then decided to use a statistical method that yields the probability of a system being stable for a given period of time, based on the planets' mutual separations<sup>58</sup>. Using the masses and semi-major axes in Table 1, we calculated the separations between all adjacent pairs of planets in units of their mutual Hill spheres<sup>58</sup>. We found an average separation of  $10.5 \pm 1.9$  (excluding planet h), where the uncertainty is the r.m.s. of the six mutual separations. We computed that TRAPPIST-1 has a 25% chance of suffering an instability over 1 Myr, and an 8.1% chance of surviving for 1 billion years (Gyr), in line with our  $n$ -body integrations.

These results, obtained by two different methods, suggest that the TRAPPIST-1 system could be unstable over relatively short timescales. However, they do not take into account the proximity of the planets to their host star and the resulting strong tidal effects that might act to stabilize the system. We included tidal effects in an ameliorated version of the Mercury package<sup>59,60</sup>, and found that they markedly enhance the system's stability. However, the disruption is only postponed by tides in most simulations, and further investigations are needed in order to better understand the dynamics of the system. In general, the stability of the system appears to be very dependent on the assumptions of the orbital parameters and masses of the planets, and on the inclusion or exclusion of planet h and on its assumed orbital period and mass. It is also possible that other, still undetected, planets help to stabilize the system. The masses and exact eccentricities of the planets remain uncertain, and our results make it likely that only a very small number of orbital configurations lead to stable configurations. For instance, mean motion resonances can protect planetary systems over long timescales<sup>61</sup>. The system clearly exists, and it is unlikely that we are observing it just before its catastrophic disruption, so it is probably stable over a long timescale. These facts and the results of our dynamical simulations indicate that, given enough data, the very existence of the system should bring strong constraints on its components' properties—their masses, orbital elements and tidal dissipation efficiencies, which are dependent on the planets' compositions, mutual tidal effects of the planets, mutual inclinations, the orbit of planet h, the existence of other, maybe not transiting planets, and so on.

**Code availability.** The conversion of the UT times of the photometric measurements to the BJD<sub>TDB</sub> system was performed using the online program created by J. Eastman and distributed at <http://astroutils.astronomy.ohio-state.edu/time/utc2bjd.html>. The MCMC software used to analyse the photometric data is a custom Fortran 90 code that can be obtained from M.G. on reasonable request. The  $n$ -body integration codes TTVFast, TTVFaster, and Mercury are freely available online at <https://github.com/kdeck/TTVFast>, <https://github.com/ericagol/TTVFaster>, and <https://github.com/smirik/mercury>. To realize Fig. 2a, we relied on TEPCAT, an online catalogue of transiting planets maintained by J. Southworth (<http://www.astro.keele.ac.uk/jkt/tepcat/>).

**Data availability.** The Spitzer data that support our findings are available from the Spitzer Heritage Archive database (<http://sha.ipac.caltech.edu/applications/Spitzer/SHA>). Source Data for Fig. 1 and Extended Data Figs 1–4 are available online. The other datasets generated and/or analysed during the present study are available from M.G. on reasonable request.

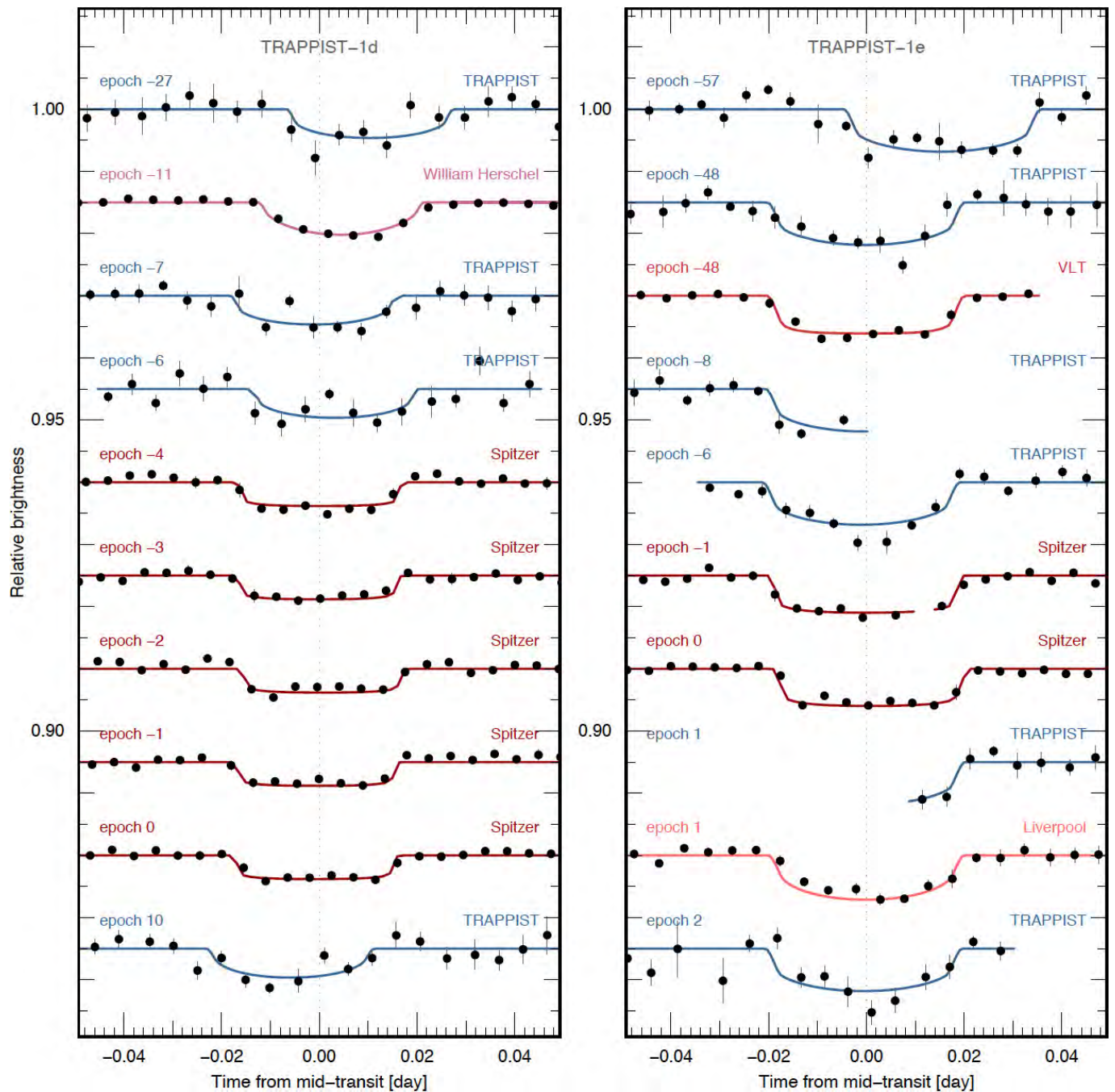
- Gillon, M. *et al.* TRAPPIST: a robotic telescope dedicated to the study of planetary systems. *EPJ Web Conf.* **11**, 06002 (2011).
- Jehin, E. *et al.* TRAPPIST: TRAnsiting Planets and Planetesimals Small Telescope. *Messenger* **145**, 2–6 (2011).
- [http://www.orca.ulg.ac.be/TRAPPIST/Trappist\\_main/Home.html](http://www.orca.ulg.ac.be/TRAPPIST/Trappist_main/Home.html)
- Pirard, J.-F. *et al.* HAWK-I: a new wide-field 1- to 2.5  $\mu$ m imager for the VLT. *Proc. SPIE* **5492**, 1763–1772 (2004).
- Casali, M. *et al.* The UKIRT IR Wide-Field Camera (WFCAM). In *The New Era of Wide-Field Astronomy* (eds Clowes, R., Adamson, A. & Bromage, G.) 357–363 (ASP Conf. Series Vol. 232, 2001).
- Benn, C., Dee, K. & Agócs, T. ACAM: a new imager/spectrograph for the William Herschel Telescope. *Proc. SPIE* **7014**, 70146X (2008).
- <http://telescope.livjm.ac.uk/TellInst/Inst/IOO/>
- <http://shoc.sao.ac.za/Documents/ShocnHelpful.pdf>
- Stetson, P. B. DAOPHOT—a computer program for crowded-field stellar photometry. *Publ. Astron. Soc. Pacif.* **99**, 191–222 (1987).
- Fazio, G. G. *et al.* The Infrared Array Camera (IRAC) for the Spitzer Space Telescope. *Astrophys. J. Suppl. Ser.* **154**, 10–17 (2004).
- Ingalls, J. G. *et al.* Intra-pixel gain variations and high-precision photometry with the Infrared Array Camera (IRAC). *Proc. SPIE* **8442**, <http://dx.doi.org/10.1117/12.926947> (2012).
- Knutson, H. A. *et al.* The 3.6–8.0  $\mu$ m broadband emission spectrum of HD 209458b: evidence for an atmospheric temperature inversion. *Astrophys. J.* **673**, 526–531 (2008).
- Gillon, M. *et al.* Search for a habitable terrestrial planet transiting the nearby red dwarf GJ 1214. *Astron. Astrophys.* **563**, A21 (2014).
- Eastman, J., Siverd, R. & Gaudi, B. S. Achieving better than 1 minute accuracy in the heliocentric and barycentric Julian dates. *Publ. Astron. Soc. Pacif.* **122**, 935–946 (2010).
- Mandel, K. & Agol, E. Analytic light curves for planetary transit searches. *Astrophys. J.* **580**, L171–L175 (2002).
- Schwarz, G. E. Estimating the dimension of a model. *Ann. Stat.* **6**, 461–464 (1978).
- Filippazzo, J. C. *et al.* Fundamental parameters and spectral energy distributions of young and field age objects with masses spanning the stellar to planetary regime. *Astrophys. J.* **810**, 158 (2015).
- Claret, A. A new non-linear limb-darkening law for LTE stellar atmosphere models. Calculations for  $-5.0 \leq \log[M/H] \leq +1$ ,  $2000\text{K} \leq T_{\text{eff}} \leq 5000\text{K}$  at several surface gravities. *Astron. Astrophys.* **363**, 1081–1190 (2000).
- Claret, A. & Bloemen, S. Gravity and limb-darkening coefficients for the Kepler, CoRoT, Spitzer, uvby, UBVRJHK, and Sloan photometric systems. *Astron. Astrophys.* **529**, A75 (2011).
- Gelman, A. & Rubin, D. B. Inference from iterative simulation using multiple sequences. *Stat. Sci.* **7**, 457–472 (1992).
- Deck, K. M. *et al.* TTVFast: an efficient and accurate code for transit timing inversion problems. *Astrophys. J.* **787**, 132 (2014).
- Chambers, J. E. A hybrid symplectic integrator that permits close encounters between massive bodies. *Mon. Not. R. Astron. Soc.* **304**, 793–799 (1999).
- Agol, E. & Deck, K. M. Transit timing to first order in eccentricity. *Astrophys. J.* **818**, 177 (2016).
- Deck, K. M. & Agol, E. Transit timing variations for planets near eccentricity-type mean motion resonances. *Astrophys. J.* **821**, 96 (2016).
- Levenberg, K. A method for certain problems in least squares. *Q. Appl. Math.* **2**, 164–168 (1944).
- Nelder, J. A. & Mead, R. A simplex method for function minimization. *Comput. J.* **7**, 308–313 (1965).
- Hanno, R. & Tamayo, D. WHFast: a fast and unbiased implementation of a symplectic Wisdom-Holman integrator for long-term gravitational simulations. *Mon. Not. R. Astron. Soc.* **452**, 376–388 (2015).
- Pu, B. & Wu, Y. Spacing of Kepler planets: sculpting by dynamical instability. *Astrophys. J.* **807**, 44 (2015); erratum **819**, 170 (2016).
- Bolmont, E. *et al.* Formation, tidal evolution, and habitability of the Kepler-186 system. *Astrophys. J.* **793**, 3 (2014).
- Bolmont, E. *et al.* Mercury-T: a new code to study tidally evolving multi-planet systems. Applications to Kepler-62. *Astron. Astrophys.* **583**, A116 (2015).
- Deck, K. M., Payne, M. & Holman, M. J. First-order resonance overlap and the stability of close two-planet systems. *Astrophys. J.* **774**, 129 (2013).



**Extended Data Figure 1 | Light curve of a triple transit of planets c, e and f.** The black points show the differential photometric measurements extracted from VLT/HAWK-I images taken on 11 December 2015, with the formal  $1\sigma$  errors shown as vertical lines. The best-fit triple-transit model is shown as a red line. Possible configurations of the planets relative

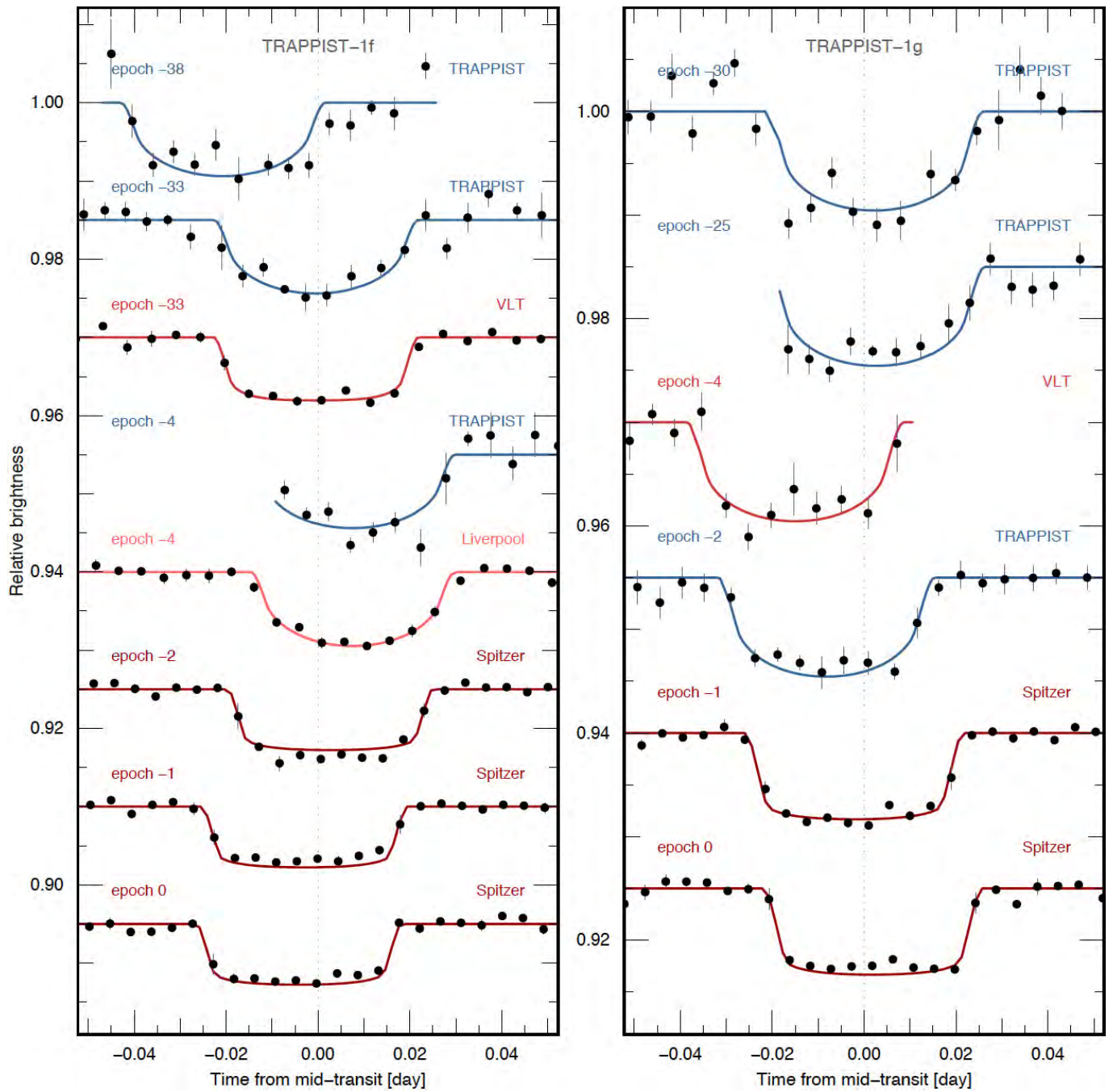
to the stellar disc are shown below the light curve for three different times (red, planet c; yellow, planet e; green, planet f). The relative positions and sizes of the planets, as well as the impact parameters, correspond to the values in Table 1.



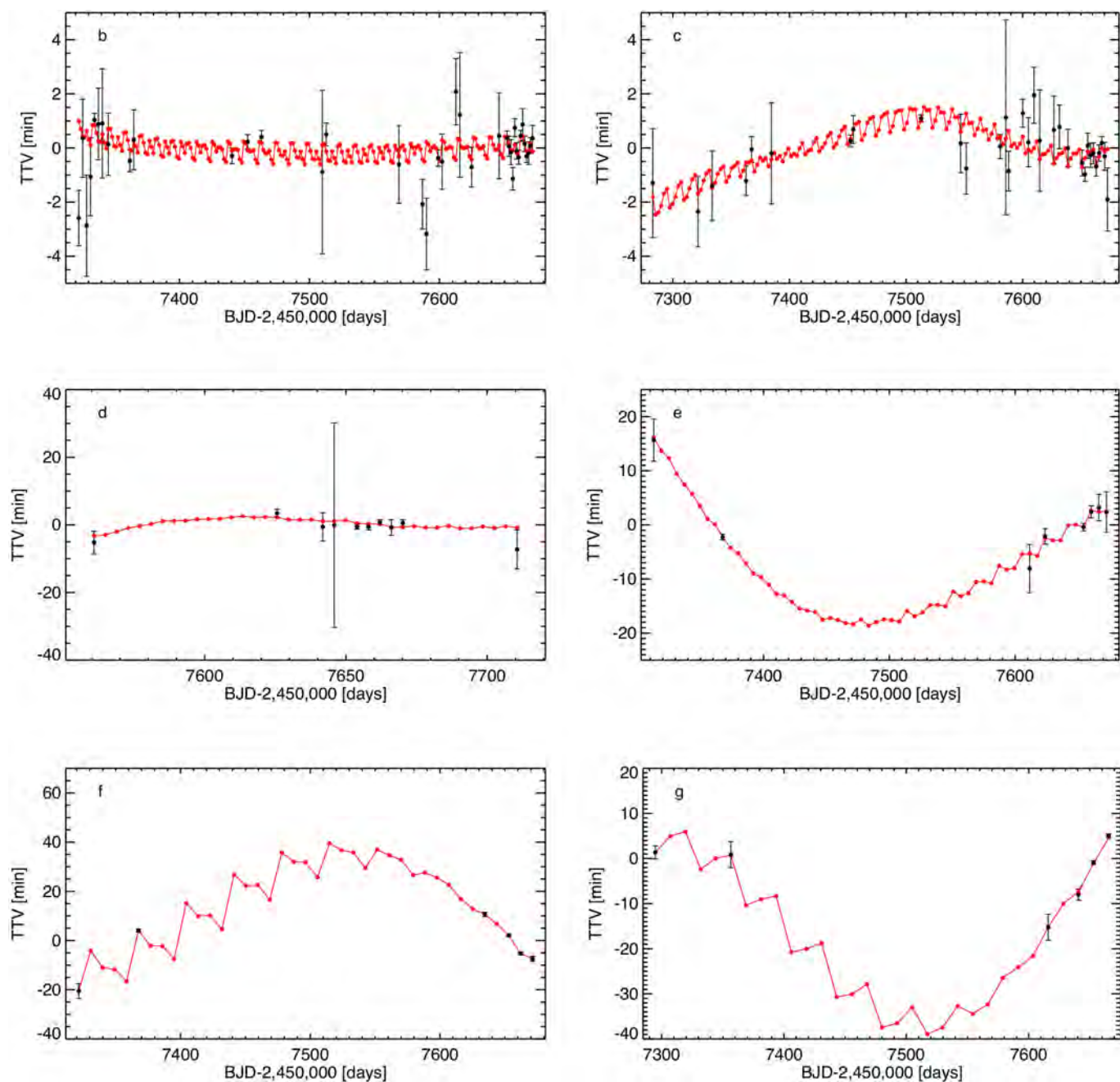


**Extended Data Figure 2 | Transit light curve for planets d and e.** The black points show the photometric measurements, binned per 0.005 days (7.2 min). The error for each bin (shown as a vertical line) was computed as the  $1\sigma$  error on the average. These light curves are divided by their best-fit instrumental models and by the best-fit transit models of other

planets (for multiple transits). The best-fit transit models are shown as solid lines. The light curves are period-folded on the best-fit transit ephemeris given in Table 1, their relative shifts on the x-axis reflecting TTVs due to planet–planet interactions (see text). The epoch of the transit and the facility used to observe it are indicated above each light curve.



Extended Data Figure 3 | Transit light curves for planets f and g. As for Extended Data Fig. 2, but for planets f and g.



**Extended Data Figure 4 | TTVs measured for planets b, c, d, e, f and g.** For each planet, the best-fit TTV model computed with the  $n$ -body numerical integration code Mercury<sup>52</sup> is shown as a red line. The  $1\sigma$  errors of the transit timing measurements are shown as vertical lines.



Extended Data Table 1 | Summary of the observation set used

Facility/instrument	Number of hrs	Year(s)	Number of light curves	Filter/grism	Number of transits
TRAPPIST-South	677.9	2013 2015 2016	214	I+z	b: 13, c: 1, d: 3, e: 5, f: 3, g: 4
Spitzer/IRAC	476.8	2016	30	4.5 $\mu\text{m}$	b: 16, c: 11, d: 5, e: 2, f: 3, g: 2, h: 1
TRAPPIST-North	206.7	2016	75	I+z	b: 4, c: 3, e: 1
LT/IO:O	50.3	2016	10	z'	b: 1, c: 1, e: 1, f: 1
UKIRT/WFCAM	34.5	2015 2016	9	J	b: 4, c: 3
WHT/ACAM	25.8	2016	4	I	b: 1, c: 1, d: 1
SAAO-1m/SHOC	10.7	2016	5	z'	None
VLT/HAWK-I	6.5	2015	2	NB2090	b: 1, c: 1, e: 1, f: 1
HCT/HFOSC	4.8	2016	1	I	b: 1
HST/WFC3	3.9	2016	1	G141 (1.1-1.7 $\mu\text{m}$ )	b: 1, c: 1

For each facility/instrument, the following parameters are given: the effective number of observations (not accounting for calibration and overhead times), the year(s) of observation, the number of resulting light curves, the used filter or grism, and the number of transits observed for the seven planets, TRAPPIST-1b, c, d, e, f, g and h.